X-RAY DIFFRACTION AND ELECTRON MICROSCOPE STUDY OF PHASE SEPARATION IN ROD OUTER SEGMENT PHOTORECEPTOR MEMBRANE MULTILAYERS

SOL M. GRUNER
Department of Physics, Princeton University, Princeton, New Jersey 08544

KENNETH J. ROTHSCHILD
Departments of Physics and Physiology, Boston University, Boston, Massachusetts 02115

NOEL A. CLARK
Department of Physics, University of Colorado, Boulder, Colorado 80309

ASTRACT Phase separation in artificially stacked multilayers of isolated bovine retinal rod outer segment (ROS) membranes has been examined via x-ray diffraction and electron microscopy. Specimens were prepared by isopotential spin drying followed with partial hydration by equilibration against moist gas streams. Upon dehydration, the multilamellar membrane phase assumes a binary phase composition consisting of concentrated protein-containing lamellae interspersed with microdomains of hexagonally packed tubes of lipid in a H_{II} configuration. The H_{II} lattice is geometrically coupled to the lamellar phase with one set of hexagonal crystal planes co-planar to the local membrane lamellae. The hexagonal microdomains bear a striking resemblance to the "paracrystalline inclusions" observed in fast-frozen, intact frog ROS (Corless and Costello. 1981. *Exp. Eye Res.* 32:217). The lamellar lattice is characterized by an unusually small degree of disorder. Sharp lamellar diffraction with a 120 Å unit cell is observed (at near total dehydration) to a resolution of 6 Å. A model consistent with the data is that a multilamellar array of ROS disks is stable as long as the external disk surfaces are kept sufficiently far apart. If the distance between the membranes is allowed to shrink below a certain critical value, the disk lipids spontaneously convert to a nonbilayer phase. This suggests that the structure of the ROS is stabilized by an internal framework that acts to keep the disks apart from one another and from the plasmalemma. Thus, the necessity of avoiding phase separations may provide a rationale for the peculiar morphology of the ROS.

INTRODUCTION

Much interest has been focused on the possibility that biological membranes can exist under some conditions in a nonbilayer configuration (Cullis and DeKruijff, 1979). It is clear from a number of studies performed on pure phospholipid systems that a multitude of nonbilayer phases exist (Luzzati, 1968). The native lipids from photoreceptor membranes have been shown to exist in the hexagonal H_{II} phase above 30°C (DeGrip et al., 1979 *a*). Evidence has also been presented recently that nonbilayer lipid phases exist in the native rod outer segments (Corless and Costello, 1981). The existence of nonbilayer phases of membranes has been suggested as a mechanism for vesicle fusion and cell division (see, for example, Cullis and DeKruijff, 1979). In addition, lateral phase separation of membrane constituents has been observed in many membranes in response to changes in hydration, temperature, and ionic strength (Quinn and Chapman, 1980). An understanding of the organization of the lipid and protein components in membrane multilamellar arrays is particularly important. Biophysical methods, including x-ray diffraction, scanning calorimetry, NMR, Raman and infrared spectroscopy, can be applied to multilamellar arrays to probe membrane structure. Few studies, however, have examined the phase composition of arrays of native membranes.

In this article we report on an electron microscope and x-ray diffraction study of bovine rod outer segment (ROS) disk membrane incorporated into multilamellar arrays via the isopotential spin-dry method (Clark et al., 1980; Rothschild et al., 1980 *a–c*). Our long-range goal is to produce highly ordered arrays suitable for high-resolution x-ray diffraction analysis. Although the intact ROS is remarkable among biological structures for the regularity in the spacings of the disks, it is quite disordered when considered in terms of the periodicity required for high resolution x-ray diffraction (Schwartz et al., 1975). Furthermore, it is desirable to examine the diffraction from chemically modified disks. It is difficult to modify disks in the intact ROS. These difficulties can be circumvented by isolating the

disks and reordering them into a multilamellar array (Santillan, 1975). Selective dehydration can then be used to shrink the fluid layers and produce very well ordered specimens. Although this allows collection of x-ray diffraction data to high resolution, it also introduces an additional problem: the lamellar lattice becomes unstable at low water content, and phase separation occurs (Barry, 1979; Gruner et al., 1980; 1982). This feature was recognized early on by most of the x-ray workers dealing with isolated disk preparations because the diffraction could not be indexed on a single Bragg lattice.[1] Phase separation has become the major impediment to obtaining a high-resolution electron-density profile of the isolated disk. This difficulty is not unique to ROS disks; it is a general problem often encountered in dealing with multilayer specimens. The purpose of this article is to provide information on the composition of the phase-separated regions in isolated disk multilayers. As we shall discuss, we believe this information relates directly to understanding the overall organization of the lipids and rhodopsin in the intact ROS. Furthermore, it sheds light on the nature of the H_{II} phase in biomembranes. Finally, an understanding of the phase separation that occurs when disk multilayers are prepared can aid in elucidating the structure of rhodopsin via x-ray diffraction.

METHODS

Specimen Preparation

Native photoreceptor membrane was incorporated into multilamellar arrays by the isopotential spin-dry technique (Clark et al., 1980). Photoreceptor disk membranes were isolated from frozen bovine retinas (Hormel, Inc., Austin, MN) using sucrose density centrifugation (DeGrip et al., 1979 *b*). Isolated disks were washed three times in doubly distilled deionized water and, finally, resuspended in distilled water. The 280–500 nm optical density ratio of the material was 2.0 to 2.2. 1 ml of this suspension, with an optical density of 0.75 OD at 500 nm, was spun onto Saran Wrap (Dow Chemical Co., Indianapolis, IN) in an isopotential centrifugation cell for 15 h at 11,000 rpm. The resulting arrays have been studied using UV-visible and Fourier transform infrared spectroscopy (Rothschild et al., 1980 *a–c*) and have been shown to exhibit regenerability with 11-*cis* retinal. Furthermore, the arrays can be fully bleached >90% relative humidity. The disk isolation and array preparation were done in the dark or under dim deep red light.

For the purpose of freeze fracture, the arrays were scraped from either plastic or glass cover slips, in room light. At low humidity the arrays crack into small fragments with this procedure; however, at high humidity 0.5 cm^2 pieces could be removed. These pieces had a tendency to curl into cylinders which were placed on copper hats and glued in place with a second hat using Gelvatol (Monsanto Co., St. Louis, MO). This was then frozen for 15 s in freon at −160°C and finally immersed in liquid nitrogen. Freeze-fracture was performed with a Balzers 301 apparatus (Balzers, Hudson, NH) using the double-replica method and replicas prepared using standard procedures (Raviola and Raviola, 1981). Electron microscopy was performed with a Philips 3,000 electron microscope (Philips Electronic, Mahwah, NJ). Based on absorption measurements made in the visible, the rhodopsin in the photoreceptor membrane films was predominantly in the Meta I state.

For the purpose of x-ray diffraction analysis, photoreceptor membrane arrays were prepared on Saran Wrap or aluminum foil, as described above. Specimens were either used within 24 h or stored in light-tight nitrogen-filled bottles under refrigeration, until needed. When stored in this manner, the specimens were stable for weeks, although good practice dictated their use as soon as feasible. Lipid analysis using HPLC on lipid extracted from stored films[2] revealed no change from the composition of fresh photoreceptor membrane. All x-ray diffraction experiments were done on dark-adapted specimens.

Nickel-filtered CuKα (λ = 1.54 Å) x-rays were generated on a Rigaku Rotaflex rotating anode x-ray generator (Rigaku/USA, Inc., Danvers, MA) at a loading of 50 kV and 55 mA. X-rays were line-focused using single mirror Franks' optics. The foreshortened (6° take-off angle), focused linewidth at the detector was, typically, 0.2 mm. Slit-collimation was used to set the height of the beam between 0.2 and 3.0 mm. The x-ray camera was configured asymmetrically (source to mirror:mirror to detector-distance ratio of ~1:3) to minimize the beam width at the sample because the samples were only 10–20 μm thick (a typical sample mass in the beam was 10–50 μg). Scattered x-rays were detected either on stacks of Kodak No-screen x-ray film (Eastman Kodak Co., Rochester, NY) or on a quantum-limited image-intensified slow-scan TV detector. This detector has been described in detail elsewhere (Reynolds et al., 1976, 1977, 1978; Gruner, 1977). The speed advantage of the TV detector (typically, a factor of 50–100 over x-ray film) allowed tracking of the changes in the diffraction as the specimens were hydrated or dehydrated. The primary limitation of the TV detector is its spatial resolution. Consequently, high-resolution detail was detected on x-ray film. Comparison of sequences of TV detector patterns before and after exposure of the film served to check on the stability of the specimens.

Specimens were cut into strips a few millimeters wide and wrapped around the outside of a section of an aluminum cylinder 2.5 cm in diameter. The cylindrical section was then advanced into the x-ray beam so that the beam tangentially grazed the specimen and was parallel to the multilayer surface. Specimens were enclosed in a small temperature-regulated chamber (4°C) through which moist helium was circulated. The water content of the specimen was varied by equilibrating the specimen at various humidities. A humidity generator (Gruner, 1981) allowed precise, quantitative control of the humidity of the helium circulated through the specimen chamber. The chamber was equipped with mylar vacuum-tight x-ray windows and was, in turn, enclosed in a light-tight vacuum housing (Gruner, 1977) to minimize air attenuation and scattering of the x-rays.

Specimen alignment was conveniently performed with the TV detector: typically three or four orders of diffraction were visible to the eye viewing the intensifier output when the specimen was translated into the beam.

Throughout this paper, the resolution, d, is given by $s = 1/d = (2\sin\theta)/\lambda$, where 2θ is the angle between the incident and diffracted x-rays and λ is the x-ray wavelength.

RESULTS

Electron Microscopy

A typical transmission electron micrograph of a replica of a freeze-fractured photoreceptor membrane film is shown in Fig. 1. The picture is characterized by several distinct regions, denoted *I–IV* in Fig. 1, which were observed to varying extents in all fractures:

(*I*) Layers of parallel tubes with an average spacing of 62.4 ± 1.0 Å, as determined by optical diffraction. In many cases these tubes curl into fingerprint type figures. These figures bear strong resemblance to features seen in fast-frozen intact ROS (Corless and Costello, 1981). These

[1]Santillan, G., J. K. Blaisie, and H. Saibil, personal communication.

[2]DeGrip, unpublished data.

regions also resemble strongly the H_{II} phase observed in pure and mixed lipid systems as studied extensively by several groups (Cullis and deKruijff, 1979; Deamer et al., 1970).

(*II*) Clustered particles on the order of 100 Å in diameter. These regions appear less frequently than the apparent H_{II} phase. Based on the size and distribution of the particles these regions are likely to be rhodopsin-rich phases. Similar particles are observed in freeze fracture of native and reconstituted rhodopsin membranes (see Olive, 1980, for a review). The particle areas are smaller and occur less frequently than in native membranes.

(*III*) Regions that appear are adjacent to region *I* and display a transition from tubes to a more randomly textured surface.

(*IV*) Flat regions with little texture.

Based on the above evidence the following model is proposed: hexagonal phase-separated regions that contain mostly lipid exist adjacent to regions which are predominantly bilayer in structure. The planes of the bilayers are parallel to planes of tubes. Thus, there appears to exist a definite orientation to the hexagonal phase which is imposed by the relative orientation of the bilayer lamellae. This model is strongly supported by the x-ray diffraction studies discussed in the next section.

X-ray Diffraction

A diffraction pattern of isolated disks prepared by the spin-dry method is shown in Fig. 2. On the original negative, the lamellar reflections are seen to 6-Å resolution. The sharpness of the reflections and the lack of a nonaxially symmetric diffuse background are indicative of a well-ordered lattice. Large, uncorrelated variations in the placement of unit cells on the lattice (lattice disorder) would have been indicated by a progressive broadening and merging of the reflections (Guinier, 1963). Another type of disorder which is often seen in membrane arrays arises from a statistical variation in the composition of the unit cells (substitution disorder). In the intact ROS, this arises from variation in the widths of the fluid spaces between the disk bilayers. Substitution disorder is appreciable in many membrane multilayers (Cain, 1974; Santillan, 1975; Schwartz et al., 1975; Gruner, 1977; Herbette et al., 1977; Nelander and Blaurock, 1978; Barry, 1979). It may be recognized by modulation of the incoherent background, specifically on the lamellar axis, which lifts the zeros between diffraction peaks off the base line of the axially symmetric incoherent scatter (Schwartz et al., 1975; Nelander and Blaurock, 1978). There is little evidence of substitution disorder in Fig. 2.

As seen in Fig. 3, the reflections may be indexed with a Bragg repeat of $d = 117.3 \pm 2.2$ Å. The uncertainty in d arises almost entirely from uncertainty in the specimen to film distance. Two very weak reflections that do not fit this simple lattice are also present in this exposure at 86.1 and 21.7 Å. These are assumed to arise from a minor contaminant in the array since they do not occur in other exposures. No single lattice can simultaneously fit these reflections and the data shown in Fig. 3.

FIGURE 1 A freeze-fracture micrograph of a spin-dried isolated disk specimen, showing a fracture surface that runs generally parallel to the lamellae. The lamellae are stacked perpendicular to the sedimentation axis. See Results (Electron Microscopy) for an explanation of the micrograph features and levels. 52,500×.

Another feature of note is the diffuse, primarily equatorial, band at 10 Å. It is similar to reflections observed in diffraction from membrane multilayers of bacteriorhodopsin (Blaurock, 1975; Henderson, 1975), sarcoplasmic reticulum (Herbette et al., 1977), hydrated, isolated ROS disk multilayers (Santillan, 1975) and intact ROS (Blaurock and Wilkins, 1969). The reflection is indicative of oriented protein; it is absent in pure lipid multilayers. It is generally

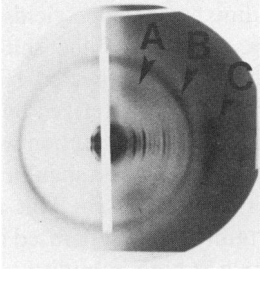

FIGURE 2 A reproduction of the top film of a 24-h x-ray film exposure of a spin-dried isolated disk specimen at 50% relative humidity. The lamellar pattern is the succession of sharp vertical lines extended along the lamellar axis. The incident line focused x-ray beam was oriented to graze the surface of the specimen tangentially. The pattern to the left of the beam stop shadow was attenuated by absorption by the substrate. Specific features are *A*, 10-Å reflection; *B*, 6-Å plastic vacuum window artifact; *C*, 5.3-Å Saran Wrap substrate artifact.

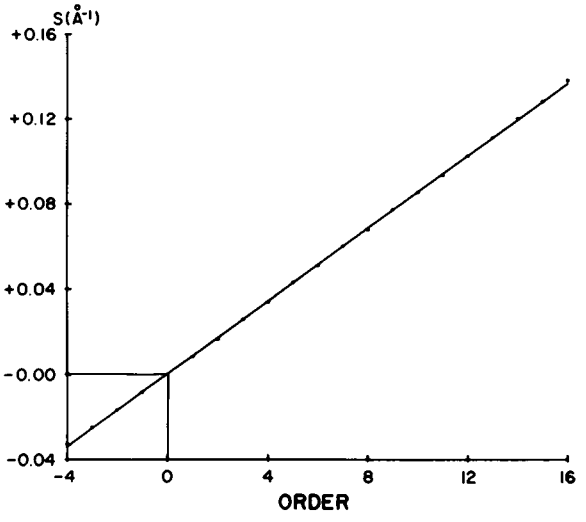

FIGURE 3 The distance $s = 2\sin\theta/\lambda$ vs. the assigned order for the first 16 orders of the exposure of Fig. 2 (higher orders do not show up well in the microdensitometer tracing). The line is the distance variation expected for a single Bragg lattice with a repeat of 117.3 Å. The line fits the data to an RMS deviation of 5.7×10^{-4} Å^{-1}.

interpreted as arising from the side-to-side packing of α-helical polypeptide chain segments or from a β-pleated sheet oriented primarily orthogonal to the membrane planes (Levine, 1973). The 10-Å x-ray reflection is consistent with the study of Rothschild et al. (1980 *c*), in which spin-dried specimens were examined via infrared spectroscopy and far-ultraviolet circular dichroism. The study concluded that the rhodopsin in the specimens consisted largely of α-helix oriented with the helical axis primarily perpendicular to the membrane plane.

The stability of the spin-dried specimens, the humidity generating system, and the speed advantage of the TV detector allowed rapid examination of the specimens over a range of hydrations. Fig. 4 illustrates how the spacings between the reflections vary as a function of the equilibrated relative humidity. If the diffraction were characterized as arising from a mosaic of lattices that swell uniformly, then the reflections would always be simply indexed to fall on a straight line whose slope yields the lattice repeat. The fact that the position of the third order (N = 3) reflection did not move as expected (Fig. 4 *b*) indicated that the lattice was not characterized by one repeat. In the TV-detector data the N = 3 reflection was seen to broaden and eventually develop a weak shoulder as the humidity increased (arrows, Fig. 4 *c*, 5 *d*). This indicated that the specimen was certainly phase separated into more than one characteristic lattice at high humidity.

The succession of film exposures of Fig. 5 shows that the specimens are phase separated at all humidities: Note the progressive broadening of the third reflection with humidity, and the separation into two reflections in the 80% relative humidity exposure (arrow, Fig. 5 *d*). The weaker of these two reflections, in fact, indexes on the fundamental lamellar repeat. The data indicate that the

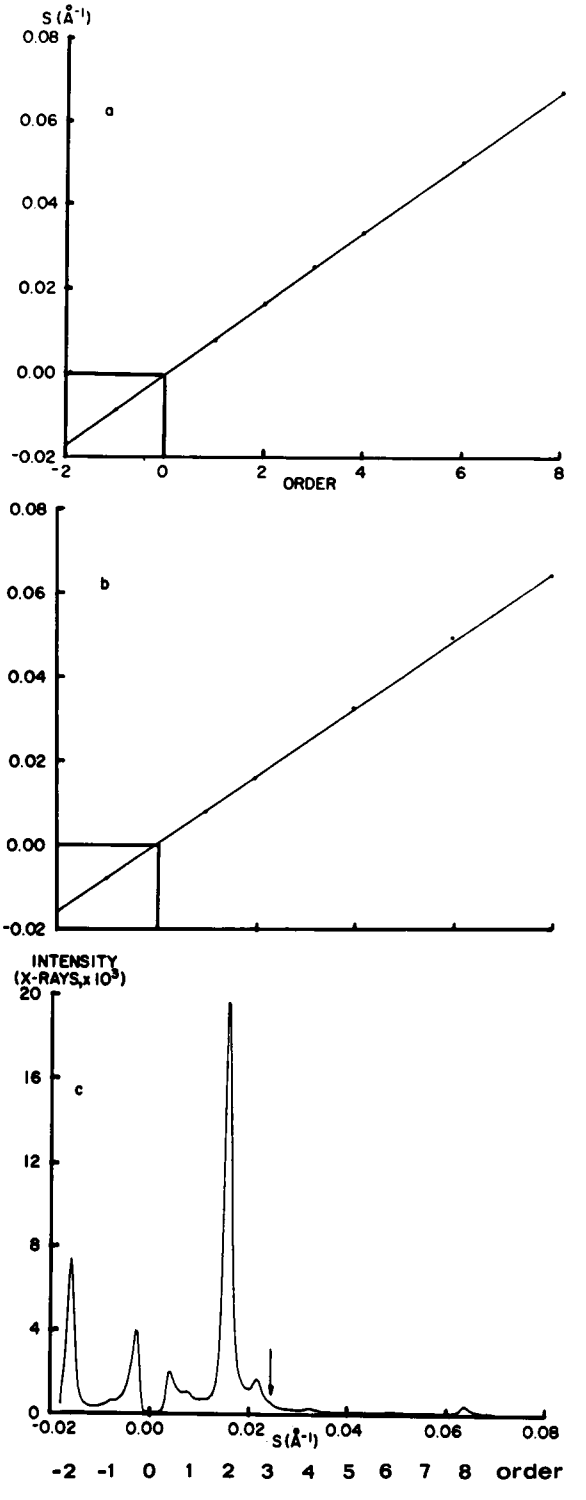

FIGURE 4 The position of the diffraction peaks vs. an index assignment, N, for a single specimen that has been equilibrated successively at 50, 90, and 50% relative humidity. The 50% data sets are drawn superimposed (*a*); hysteresis was negligible in this specimen so the drawings are indistinguishable. The strongest peaks in the vicinity for $N = 3$ and $N = 6$ at 90% relative humidity (*b*) fail to fall on the straight line required by the Bragg law if all peaks arose from a single characteristic lattice. Examination of the diffraction (*c*) indicates a very weak shoulder at the proper $N = 3$ position (arrow). From the slopes of *a* and *b*, the unit cells are 119.9 and 125.4 Å, respectively. These data are from 12-min TV-detector exposures.

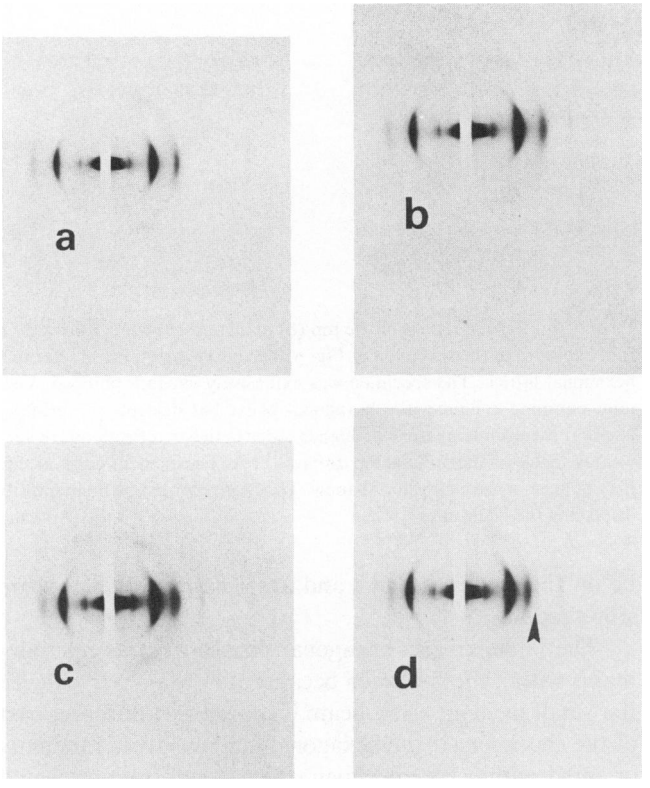

FIGURE 5 Reproductions from a succession of x-ray film exposures taken on a single specimen equilibrated at $a = 50$, $b = 60$, $c = 70$, and $d = 80\%$ relative humidity. Note the progressive broadening and eventual splitting (*d*, arrow) of the third order reflection. Also note the off-axis reflections which maintain the same distances from the origin as the darker component of the "third" reflection. These reflections are due to the phase separated hexagonal lattice. The orders to the left of the beam stop are weaker because they must go through the aluminum foil substrate. Substrate absorption artifacts are greatest for the low order reflections which have small diffraction angles. The apparent splitting of the $N = -1$ reflection (immediately to the left of the beam stop) is such an artifact; the $N = +1$ reflection is not split on any of the films. Exposure times varied from 6 to 10 h at a specimen to film distance of 390.4 mm.

specimen consists of two coexisting phases whose Bragg repeats on the lamellar axis are commensurate at low humidity. As the specimen is swollen, the two phases swell at different rates. This leads to an apparent broadening and finally a separation of the respective Bragg reflections. This conclusion is strongly supported by the weak reflections at 60° to the lamellar axis (see below). These are at the same distance from the origin as the stronger of the "third" reflections, and move with it. It is proposed that these belong to a lattice which will be denoted, from here onward, as the hexagonal phase. The remaining reflections are consistent with a single lamellar lattice and will be called the lamellar phase.

The presence of the off-axis hexagonal reflections at lower humidities is compelling evidence that the phase separation is present even at the lower humidities. There are no off-axis reflections associated with the first two reflections on the lamellar axis. Therefore, the lowest order hexagonal reflections at 50% humidity arise from a repeat

TABLE I

BASIS VECTOR LENGTHS OF THE LAMELLAR AND HEXAGONAL LATTICES FOR TWO SPECIMENS AT VARIOUS RELATIVE HUMIDITIES

Specimen	Relative humidity	Basis vector	
		Lamellar	Hexagonal
	(%)	(Å)	
A	50	117.2	46.0
A	60	120.6	47.8
A	70	122.5	50.6
A	80	123.6	54.3
B	50	124.3	51.3
B	80	131.7	62.1

Specimen A was spun from disks suspended in distilled water; Specimen B was spun in 1 mM NaCl.

(i.e., the distance between the [1,0] crystal planes) about one-third that of the lamellar lattice repeat. The real space hexagonal lattice basis vector, is then $2/\sqrt{3}$ times as long. The lamellar and hexagonal basis vector lengths for Fig. 5 are shown in Table I. These value should be taken as typical dimensions because the specimens often exhibit considerable hysteresis upon swelling and dehydrating. The incorporation of NaCl considerably increases the repeat. Even larger spacings are seen for specimens that are water dipped. Thus, the hexagonal repeat is a sensitive function of the environmental conditions of the specimen. The large (62 Å) hexagonal tube repeat seen in the freeze-fracture micrographs is presumed to be due to the hydration of the specimen when it is prepared for freeze fracture.

The off-axis reflections are more readily studied by using a point-collimated x-ray beam. The variation in diffracted intensity as a function of the azimuthal angle about the incident beam direction is shown in Fig. 6, so that the intensities of the on- and off-lamellar axis hexagonal reflections may be compared. The peaks at 0° and 180° in Fig. 6 *b* are on the lamellar axis and, consequently, also contain contributions from the lamellar lattice. However, inspection of Fig. 5 *d* suggests that the intensity of the N = 3 lamellar reflection is small compared with the intensity of the hexagonal reflection at the same location. (Note that all the peaks in Fig. 6 have the same width and, therefore, arise from lattices of comparable mosaic spread.)

The reflections of Fig. 6 (from left to right) may be indexed on a planar hexagonal array with indices $(h,k) = (1,0), (0,1), (-1,1), (-1,0), (0,-1), (1,-1)$.[3] In such an

[3]As explained in the Appendix, the $(1,-1)$ and $(0,1)$ and the $(-1,1)$ and $(0,-1)$ lattice points are mixed by the macroscopic axial asymmetry of the specimens. The index assignment given in Figs. 6 and 7 is to be understood as representing this mixing. Thus, for example, the reflection labeled $(1,-1)$ actually arises in equal parts from the $(1,-1)$ and $(0,1)$ lattice points. Reflection mixing occurs for all reflections which are off the lamellar axis.

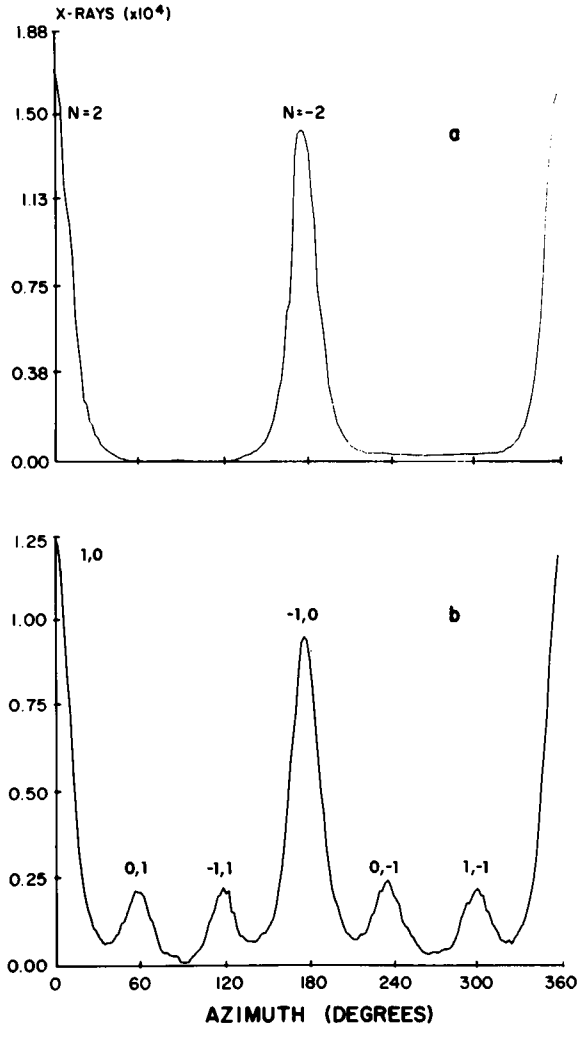

FIGURE 6 The x-ray intensity at constant reciprocal radius vs. azimuthal angle about the incident beam for a 30 min point-collimated TV-detector exposure. The data was integrated in cells 2° long between 0.00246 and 0.00254 $Å^{-1}$ for (*a*) and 0.00388 and 0.00418 $Å^{-1}$ for (*b*), corresponding to the positions of the second and third peaks on the lamellar axis. The lamellar axis cuts this integration at 0° and 180°. The 180° peaks are smaller due to substrate absorption. This specimen was kept in vacuum (see caption Fig. 7).

array, the distance of the (h, k)th reflection from the origin is proportional to

$$(h^2 + hk + k^2)^{1/2}$$

Thus, reciprocal space distances of successively higher order reflections should conform to the relative ratios of

$$1 : \sqrt{3} : \overline{7} \ldots .$$

Higher order reflections may be seen in Fig. 7. The (1,1), (−2,1), (−1,−1), and (2,−1) reflections are predicted to be at 30° to the lamellar axis and $\sqrt{3}$ further from the origin than the (1,0). Both predictions are borne out, confirming the proposed indexing of the hexagonal reflections. The (−1,2) and (1,−2) reflections are predicted to

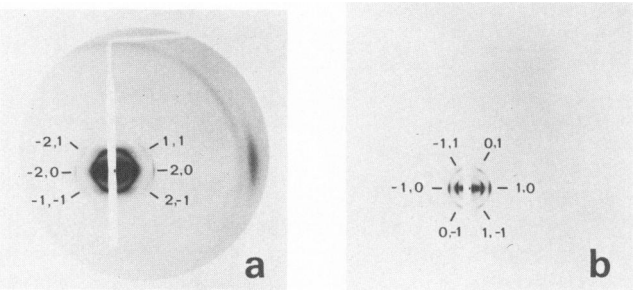

FIGURE 7 Reproductions of the top (*a*) and third (*b*) films from a 37 h film exposure of the specimen of Fig. 6. The index assignments refer to a hexagonal lattice. The specimen was extensively vacuum pumped. Vacuum pumping enhances the hexagonal phase but disrupts the primary lamellar membrane phase. The higher order lamellar reflections are very weakly visible on the original top film to ~11 Å. The incident beam profile may be seen in the beam stop shadow. This was recorded by momentarily displacing the beam stop.

be on the equatorial axis and are obscured by the beam stop shadow.

The lamellar and hexagonal phases exist as microdomains within the specimen because they are observed even if a small incident x-ray beam is moved to a different part of the specimen. If the hexagonal domains were randomly oriented within the specimen, then the diffraction would present rings similar to the powder pattern of a crushed hexagonal crystal. This is not the case: the hexagonal reflections are always oriented with respect to the lamellar reflections. Similar hexagonal reflections were observed by Finean and co-workers in a variety of dried membranes (Finean et al., 1968). They suggested that the reflections were related to an oriented, separated lipid phase.

DISCUSSION

A model consistent with all of the data is one in which the specimen is composed of a mosaic of mutually constrained lamellar and hexagonal microdomains. The electron micrographs suggest that the hexagonal domains are hexagonally packed tubes of lipid with the lipid head-groups clustered toward the centers of the tubes (H_{II} lipid). Macroscopically, the specimens are axially symmetric about the sedimentation axis; consequently, the directions of the lipid tube axes must be distributed uniformly about the sedimentaion axis. (Axial symmetry is confirmed by optical birefringence measurements and by the fact that the x-ray diffraction is invariant with respect to axial rotations of the specimen.) An insightful mental picture of such a structure may be visualized by considering what has been termed the "spaghetti-on-the-floor" model: Imagine gluing cooked spaghetti strands side by side into a hexagonally packed bundle. The spaghetti strands represent the lipid tubes and a bundle of packed strands represents a hexagonal domain. Next, imagine spacing a number of such bundles on the floor. The floor represents the surface of a local lamellar membrane array. If many bundles are

set down at random, the directions the bundles of spaghetti take will be uniformly distributed in the plane of the floor. The spaghetti bundles are not rigid: they may curve and wander in the plane of the floor. Locally, however, the cross-section of a given bundle is a well-defined two-dimensional hexagonal lattice.

The x-ray data demonstrate that the hexagonal and lamellar domains have comparable mosaic spreads and are oriented with a lowest order set of hexagonal domain crystal planes parallel to the multi-layer lamellae. These features can be incorporated in our model in a very simple way. Instead of dropping preglued bundles of spaghetti onto the floor, imagine building the bundles on the floor, layer by layer, from the floor up. This ensures that the layer of spaghetti in contact with the floor forms a plane layer parallel to the floor. The mutual orientation will then be preserved up through the hexagonal stacking. Moreover, if the floor is warped and buckled the distribution of angles the floor makes with a level floor (the analogue of the mosaic spread) will be represented in the hexagonal bundle.

The spaghetti-on-the-floor model can be used to predict the relative intensities of the off- and on-lamellar axis hexagonal reflections. The ratio of intensities for the (0,1) and (1,0) reflections is computed in the Appendix and is given by Eq. 2. For the data of Fig. 6, the mean value of the ratios of the peak intensities of the on-axis hexagonal reflections to each of its off-axis neighbors is 4.9 ($\pm$0.3 SEM). The mean value of the left-hand side of Eq. 2 for the (0,1) and (1,0) peaks is 4.9.

The x-ray and electron microscope evidence unequivocally demonstrates the specimen is composed of hexagonal and lamellar microdomains. The composition of the domains must be inferred from similarities to other membranes and, consequently, is less certain. The appearance of the hexagonal phase in the freeze-fracture micrographs is extremely similar to H_{II} lipid (Deamer et al., 1970; Gulik-Krzywicki, 1975; DeGrip et al., 1979). The range of basis vector lengths is consistent with those observed for a variety of H_{II} lipids (Deamer et al., 1970) and, in particular, is within the range observed for H_{II} configurations of water and various phosphatidylethanolamines (Shipley, 1973). The ROS contains a substantial concentration of unsaturated phosphatidylethanolamine (Anderson et al., 1975; Miljanich et al., 1981). This is significant because Cullis and DeKruijff (1978) have found that phosphatidylethanolamine from many species exhibits reversible bilayer to H_{II} phase transitions in all the cases examined. Finally, DeGrip et al. (1979) found that isolated bovine ROS lipids exhibit both lamellar and H_{II} phases at 37°C. We conclude that the hexagonal phase we observe is likely to be H_{II}.

The small diameter of the hexagonal phase tubes and the absence of particles in the freeze-fracture micrographs argue against the presence of protein in the hexagonal phase. The orientation of the 10-Å equatorial diffraction band suggests peptide α-helix or β-pleated structures are oriented largely orthogonal to the lamellar planes. Rothschild et al. (1980 *a,c*) found the presence of normally oriented α-helix by infrared and ultraviolet examinations of the spin-dried specimens. In conjunction with studies that indicate that rhodopsin contains extensive oriented α-helix (Santillan, 1975; Rothschild et al., 1976; Osborne and Nabedryk-Viala, 1977; Gruner et al., 1978; Chabre, 1978; Michel-Villaz et al., 1979; Litman, 1979), this suggests that rhodopsin is predominantly confined to the lamellar phase. Particles resembling protein in bilayers appear in the freeze-fracture micrographs, but considerably less frequently than flat, smooth-textured regions. A similar situation has been encountered in other membranes that have undergone lateral phase separation (Wunderlich et al., 1975; Borochov and Shinitzky, 1976; Armond and Staehelin, 1979). In these cases, the paucity of particle-rich regions was attributed to vertical displacement of protein out of the fracture plane.

The hexagonal and lamellar phases cannot be considered independently since mass exchange must occur between the two phases. Spin-dried arrays are made by vacuum dehydrating centrifugally sedimented vesicles. Initially, the array consists almost entirely of a disordered lamellar phase. The formation of the nonbilayer phase proceeds at the expense of the lamellar phase at some critical stage in the dehydration process. We will argue that asymmetric properties of the bilayer determine how the process proceeds.

Consider the continuum of states of an isolated disk specimen as it goes from a layering of disks with thick fluid spaces to a dried array. Gruner et al. (1980; 1982; Barry, 1979) have examined the x-ray diffraction from slowly drying, highly hydrated disk multilayers. Initially, the unit cell profile consists of two predominantly symmetric bilayers separated by wide fluid spaces. The symmetry of the low-resolution bilayer profiles indicates that mass is distributed largely uniformly across the thickness of the bilayer; this is consistent with the bilayer profiles of intact frog rods (see Blaurock, 1977, for a summary). As the multilayer slowly dehydrates the fluid spaces are of equal thicknesses and contract uniformly with no appreciable change in the bilayer profile. The uniform contraction indicates that the forces that stabilize the width of the fluid layers do so with comparable strength on either side of the bilayer. When the unit cell dimension approaches 150 Å a dramatic change occurs in the diffraction patterns. First, the odd-number diffracted orders increase rapidly in intensity, indicating the mass distribution in the unit cell becomes asymmetrical. At about the same time, the specimen begins to phase separate, as indicated by the appearance of additional reflections on the lamellar axis. The exact structure of the initial phase-separated state has not yet been resolved. The phase separation complicates the diffraction patterns and precludes a simple profile analysis. However, it demonstrates that a reorganization of the unit cell has occurred. Further dehydration results in a further

increase in the intensity of the odd numbered orders of the primary phase and a decrease in the disorder of both phases. In specimens discussed in this paper, which have been spin dried in distilled water, the process is carried to the extreme of very well organized phases and a minimum lamellar unit of just under 120 Å.

The asymmetrization of the mass of the unit cell that occurs at roughly 150 Å is an indication of asymmetric properties of the bilayer surfaces. The disk bilayer is known to have an asymmetric lipid composition (Raubach et al., 1974; Crain et al., 1978; Miljanich et al., 1981). Additionally, proteolytic digestion and labeling studies have demonstrated the chemical asymmetry of the disk proteins (see Olive, 1980, for a review). Different surface interactions on the two sides of the bilayer can lead to mass asymmetry via differences in the intra- vs. intervesicle fluid thicknesses, interdigitation of membrane surface features, or redistribution of components across the bilayer thickness.

As discussed above, 150 Å appears to be a crucial unit cell dimension for the onset of disk phase separation. In this regard, Corless and Costello (1981) have recently shown that paracrystalline inclusions are present in ultra-rapidly frozen frog ROS. Control experiments were performed that suggested that the inclusions were present in the native system and were not experimentally induced artifacts. The similarity of their inclusions to our hexagonal domains is striking. Corless and Costello exhibit freeze-fracture electron micrograph stereo pairs of inclusions that appear oriented with respect to the disk lamellae. The inclusion repeat distances are considerably larger than our hexagonal repeats, but it must be noted that the ROS contains both ionic solutes and much water. Significantly, they also note the disk surfaces immediately adjacent to the inclusions have an anomalously small repeat of ~150 Å. The reader is referred to their paper for a discussion of the similarities of the inclusions to H_{II} lipid and the implications upon the ROS.

The phase separation that occurs at a unit cell repeat of ~150 Å may explain why the disk repeat usually encountered in intact ROS (~300 Å) is so large. This distance is maintained by some unknown mechanism that keeps the intradisk space small and the interdisk space large. This mechanism is ineffective in the hydrated isolated disk multilayers because, in this case, the intra-and intervesicle spaces are nearly equal. As discussed above, a lattice contraction below two bilayers per ~150 Å results in a phase separation. A possible function of the large interdisk space in the ROS is to avoid spontaneous phase separation. Corless and Costello (1981) may have observed local, perhaps transient, failures of the disk-separating mechanism.

The above discussion suggests a hypothesis which is consistent with the observed phase-separation phenomena. The hypothesis is that a bilayer-to-nonbilayer lipid phase transition occurs if external disk surfaces come into close proximity. It is emphasized that the validity of this hypothesis has yet to be established. It is posed here primarily to stimulate further inquiry. Implications of the hypothesis follow:

(*a*) External disk surfaces must be separated if the ROS is to maintain a bilayer organization. Internal disk surfaces are normally in close opposition; consequently, we suppose that they do not spontaneously undergo the phase transition. This might be a result of an asymmetry of lipid composition in the disk bilayer. In this regard, Crain et al. (1978) and Miljanich et al. (1981) have performed labeling studies that suggest that a major fraction of the disk phosphatidylethanolamine is in the external monolayer.

(*b*) Dehydration induces phase separation in isolated disk specimens by forcing external disk surfaces together. Normally the disks are held apart by electrostatic forces.

(*c*) Since the disk is formed by an infolding of the plasmalemma (Young, 1974), it is plausible to assume the lipids of the cytoplasmic side of the plasmalemma are compositionally similar to the outside of the disk. In this case, the disks must not touch the interior of the ROS if phase separation is to be avoided. This may explain the space that is observed between the disks and the plasmalemma (Cohen, 1972).

(*d*) DeGrip et al. (1979) have suggested that rhodopsin plays a role in stabilizing the bilayer phase. This followed from their demonstration that extracted disk lipids exhibit both lamellar and H_{II} phases. Our data imply that the presence of rhodopsin is insufficient to avoid the formation of the H_{II} phase. Rather than postulating a special role for rhodopsin in the lateral organization of the membrane, it may be sufficient to consider the effect of rhodopsin and other disk components as stabilizing in so far as they keep the membranes apart. In this regard, the discrepancies between the measurements of Deese et al. (1981) and DeGrip et al. (1979) may be a result of slightly differing experimental conditions, serving, in the former case, to keep the lipid bilayers apart.

(*e*) The hypothesis limits the mechanisms whereby a lipid molecule moves from the bilayer to the H_{II} phase. Such mechanisms are currently controversial (see, for example, Hui et al., 1981). Striking features of our data are that the hexagonal lattice is oriented with respect to the lamellar phase and has the same mosaic spread. As suggested by the spaghetti-on-the-floor model, this would follow if the hexagonal phase were to grow layer by layer from the lamellar phase, as opposed to growing from a bulk intermediate phase. The hypothesis also suggests that the H_{II} phase may not be able to form without contact between a disk surface and another disk surface or H_{II} region. In other words, a single extended disk bilayer may never be able to spontaneously convert to an H_{II} phase. Cullis and Hope (1978) have suggested a specific sequence whereby H_{II} may form at the interface between two membranes. We suggest that microscopic separation of membranes may be a novel method of phase control in living organisms.

We conclude by noting that the above findings could have direct relevance in several areas: (*a*) There exists evidence that the fusion of biomembranes and artificial membranes may proceed through the formation of a nonlamellar phase. Our work supports this picture and demonstrates that detailed information can be obtained using the approach described here about the relationship of the hexagonal and bilayer phase and the conditions that govern the transition. (*b*) While we have emphasized the importance of maintaining a critical separation distance between the disks in order to avoid formation of the hexagonal phase, it is also interesting to consider the possibility that such a bilayer-to-hexagonal phase transition triggered by the close contact of two membrane in the ROS plays some physiological role. One could speculate that the formation of Ca-Na exchange mechanisms between the intradiskal space and the external rod medium, as postulated by Schnetkamp (1980), might involve some type of transient channel formed by a fusion of the plasmalemma and disk membrane. (*c*) The utilization of multilamellar arrays of membranes illustrates their usefulness as a system to study the three-dimensional ordering and interaction of membrane components. However, since the internal array environment is far from physiological, caution should be exercised in interpreting the data.

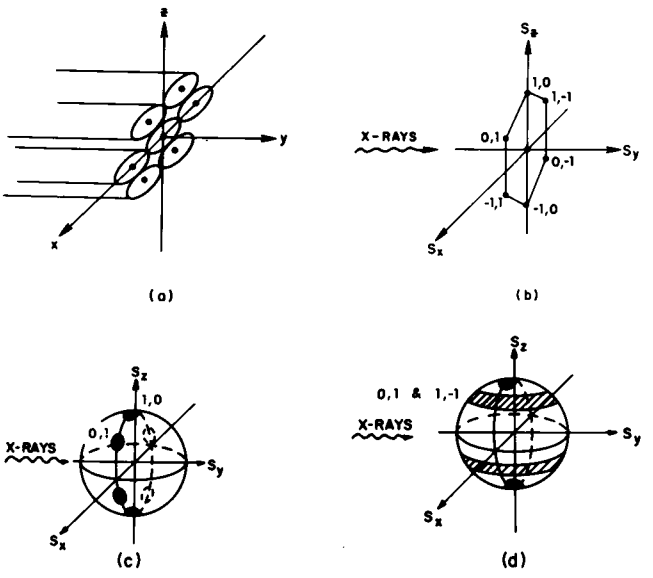

FIGURE 8 (*a*) A real-space lattice of hexagonally packed circular tubes of indefinite length extended along the *y*-axis. Only a few unit cells are shown. (*b*) The lower-most orders of the reciprocal lattice corresponding to *a*. (*c*) The reciprocal lattice after the introduction of mosaic spread. The lattice points spread into caps on the mosaic sphere. The caps have a maximum density at the original lattice points and are azimuthally symmetric about these points. (*d*) The reciprocal lattice after the further introduction of isotropy of tube orientations in the *x*-*y* plane. This follows because the specimens are macroscopically axially symmetric about the sedimentation (*z*) axis.

APPENDIX

We propose a model that accounts for the relative intensity ratios of the on- and off-lamellar axis hexagonal reflections. The model assumes that the specimen is axially symmetric about the sedimentation axis, i.e., about the line perpendicular to the mean membrane plane. The model is best first conceived as arising from an ideal hexagonal lattice. One then considers successive perturbations to this idealization to predict the observed diffraction. Consider the diffraction expected from hexagonally packed tubes of indefinite length extended along the incident beam direction (Fig. 8 *a*) taken to be along the *y*-axis. The corresponding reciprocal lattice is a hexagon of points confined to the s_x-s_z plane (Fig. 8 *b*). One takes the *z*-axis to be the sedimentation axis and then considers the effects of mosaic spread and axial symmetry. Because of mosiac spread, the reciprocal lattice is the ensemble of tilted ideal lattice points, i.e., the locus of the ideal lattice as it is rocked through all possible angles. This causes the lattice points to be spread as spherical "caps" over a sphere of disorder (Fig. 8 *c*). Since the hexagonal array of tubes is assumed to be locally tied to the host lamellar lattice, the intensity (density of points) of the caps peaks at their centers, i.e., the original ideal lattice positions. The diffraction observed implies that one of the low-order hexagonal crystal planes is parallel to the average membrane plane. The mosaic spreads of all the reflections are equal. Consequently, a single sphere of disorder characterizes the probability of angular orientation of the lattice in a given domain.

The effect of the postulate of axial symmetry is to rotate the mosaically spread lattice about the s_z-axis (Fig. 8 *d*). This corresponds to removing any bias of direction of the long axes of the hexagonally packed tubes in the membrane plane; thus, all directions in the *x*-*y* plane are equally probable. Such as axial symmetry would arise if the hexagonally packed tubes were curved and wandered over the *x*-*y* plane, as observed in the freeze-fracture micrographs. The model applies as long as the radius of curvature is large compared with the unit cell dimension. Hence, the effect of axial symmetry upon the reciprocal lattice is to further spread the density of points of the off-axis hexagonal reflections into bands of latitude about the sphere of disorder, but to leave the on-axis ("polar") reflections invariant.

The Ewald construction may be used to visualize the diffraction expected from such a reciprocal lattice. Recall that the Ewald sphere is a thin spherical shell, of radius $1/\lambda = 0.65$ Å^{-1}, centered at $s_y = -1/\lambda$. The observed diffraction is proportional to the density of the intersection of the Ewald sphere and the reciprocal lattice viewed as projected from the Ewald sphere center onto a detector plane orthogonal to the s_y-axis at a large positive value of s_y. The radius of the sphere of disorder for the first reciprocal lattice hexagon ($s_r = 1/40$ Å^{-1}) is so much smaller than the Ewald sphere that its intersection with the Ewald sphere may be approximated as the intersection with the s_x-s_z plane.

A computation of the integration over the intersection volume may now be made. We consider an integration over a small volume, V, within the intersection of the Ewald sphere and the lattice cap on the s_r axis. The volume is given by $V \simeq \Delta s_r \cdot t \cdot s_r \cdot \Delta\alpha$, where Δs_r is the radial thickness of the lattice cap, t is the thickness of the Ewald sphere, and $s_r\Delta\alpha$ is the extent along the s_x-axis (the polar angle is denoted by α). Let $I(\alpha)$ characterize the polar density distribution of the $I_{1,0}$ lattice cap. Then the diffraction at the peak of the $I_{1,0}$ reflection has intensity

$$I_{1,0} \simeq I(0)V.$$

The azimuthally integrated density of the circular band of angular width at $\alpha = 60°$ is

$$I_b = 2s_r\Delta\alpha\Delta s_r \int I(\alpha)\mathrm{d}\alpha, \qquad (1)$$

distributed over a volume of

$$V_b = 2\pi s_r \sin 60° \, s_r \, \Delta\alpha\Delta s_r.$$

The factor of 2 in Eq. 1 arises because two lattice points contribute the

reflection and the integral over $I(\alpha)$ is understood to be over the full range of α encompassing a peak.

The intensity, $I_{0,1}$, at the peak of the (0,1)-(1,−1) reflection is given by

$$I_{0,1} = I_b V / V_b.$$

Finally, the ratio of the peak intensities may be expressed in terms of the peak intensity of the (1,0) reflection and its full-width angular integration as

$$\frac{I_{0,1}}{I_{1,0}} = \frac{\int I(\alpha)\, d\alpha}{\pi I(0) \sin 60°} \quad (2)$$

As noted in the Discussion section, the data are in excellent agreement with Eq. 2.

We gratefully acknowledge the assistance of W. DeGRip, T. Fredo, G. T. Reynolds, and K. Rosen. We wish to thank the many people who have seen the data and offered fruitful suggestions.

We also thank the agencies which made this research possible: Department of Energy grant EY 76-S-02-3120 and National Institutes of Health (NIH) grant EY02679 to Dr. Gruner; Army Research (ARO) grant DAAG29-79-C-0174 to Dr. Clark; NIH grants EY02142 and EY0199 to Dr. Rothschild, who is also supported as an Established Investigator of the American Heart Association.

Received for publication 10 February 1982 and in revised form 15 March 1982.

REFERENCES

Anderson, R. E., M. B. Maude, and W. Zimmerman. 1975. Lipids of ocular tissues. X. Lipid-composition of subcellular fractions of bovine retina. *Vision Res.* 15:1087–1090.

Armond, P. A., and L. A. Staehelin. 1979. Lateral and vertical displacement of integral membrane proteins during lipid phase transition in *Anacysti nidulans*. *Proc. Natl. Acad. Sci. U. S. A.* 76:1901–1905.

Barry, D. T. 1979. Correlated x-ray diffraction analysis and electron microscopy of photoreceptor membranes. Ph.D. Thesis. Princeton University, Princeton, N.J.

Blaurock, A. E. 1975. Bacteriorhodopsin: a trans-membrane pump containing α-helix. *J. Mol. Biol.* 93:139–158.

Blaurock, A. E. 1977. What x-ray and neutron diffraction contribute to understanding the structure of the disc membrane. *In* Vertebrate Photoreception. H. D. Barlow and P. Fatt, editors. Academic Press, Inc., New York. 61–76.

Blaurock, A. E., and M. H. F. Wilkins. 1969. Structure of frog photoreceptor membranes. *Nature (Lond.)*. 223:906–909.

Borochov, H., and M. Shinitzky. 1976. Vertical displacement of membrane proteins mediated by changes in microviscosity. *Proc. Natl. Acad. Sci. U. S. A.* 73:4526–4530.

Cain, J. E. 1974. The structure of the Chromatophore membrane determined by x-ray diffraction. *Fed. Proc.* 33:1461.

Chabre, M. 1978. Diamagnetic anisotropy and orientation of α-helix in frog rhodopsin and Meta II intermediate. *Proc. Natl. Acad. Sci. U. S. A.* 75:5471–5474.

Clark, N. A., K. J. Rothschild, D. A. Luippold, and B. A. Simon. 1980. Surfaced induced orientation of multilayer membrane arrays: theoretical analysis and a new method with application to purple membrane fragments. *Biophys. J.* 31:65-96.

Cohen, A. 1972. Rods and Cones. *In* Handbook of Sensory Physiology, H. Teuber, editor. Springer-Verlag, Berlin. 8:63–110.

Corless, J. M., and M. J. Costello. 1981. Paracrystalline inclusions associated with the disk membranes of frog retinal rod outer segments. *Exp. Eye Res.* 32:217–228.

Crain, R. C., G. V. Marinetti, and D. F. O'Brien. 1978. Topology of amino phospholipids in bovine retinal rod outer segment membranes. *Biochemistry.* 17:4186–4192.

Cullis, P. R., and B. DeKruijff. 1978. The polymorphic phase behavior of phosphatidylethanolamines of natural and synthetic origin. A ^{31}P NMR study. *Biochim. Biophys. Acta.* 513:31–42.

Cullis, P. R., and B. DeKruijff. 1979. Lipid polymorphism and the functional roles of lipids in biological membranes. *Biochim. Biophys. Acta.* 559:399–420.

Cullis, P. R., and M. J. Hope. 1978. Effects of fusogenic agent on membrane structure of erythrocyte ghosts and the mechanism of membrane fusion. *Nature (Lond.)*. 271:672–674.

Deamer, D. W., R. Leonard, A. Tardieu, and D. Branton. 1970. Lamellar and hexagonal lipid phases visualized by freeze-etching. *Biochim. Biophys. Acta.* 219:47–60.

Deese, A. J., E. A. Dratz, and M. F. Brown. 1981. Retinal rod outer segment lipids form bilayers in the presence and absence of rhodopsin: a ^{31}P NMR study. *FEBS (Fed. Eur. Biochem. Soc.) Lett.* 124:93–99.

DeGrip, W. J., E. H. S. Drenthe, C. J. A. Van Echteld, B. DeKruijff, and A. J. Verkleij. 1979 *a*. A possible role of rhodopsin in maintaining bilayer structure in the photoreceptor membrane. *Biochim. Biophys. Acta.* 558:330–337.

DeGrip, W., F. J. M. Daemen, and S. L. Bonting. 1979 *b*. Isolation and purification of bovine rhodopsin. *Meth. Enzymol.* 67:301–320.

Finean, J. B., R. Coleman, S. Knutton, A. R. Limbrick, and J. E. Thompson. 1968. Structural studies of cell membrane preparations. *J. Gen. Physiol.* 51:10s–25s.

Gruner, S. M. 1977. The application of an efficient x-ray detector to diffraction from isolated rod outer segment membranes. Ph.D. Thesis. Princeton University, Princeton, NJ.

Gruner, S. M. 1981. Controlled humidity gas circulators. *Rev. Sci. Instrum.* 52:134–136.

Gruner, S. M., D. T. Barry, Geo. T. Reynolds, and J. K. Blasie. 1978. X-ray diffraction analysis of α-helix in rhodopsin. *Biophys. J. (Abstr.)*. 21:134 *a*.

Gruner, S. M., D. T. Barry, and Geo. T. Reynolds. 1980. X-ray diffraction profile study of isolated bovine rod outer segment disks. *Fed. Proc. (Abstr.)*. 39:1807.

Gruner, S. M., D. T. Barry, and Geo. T. Reynolds. 1982. Material in preparation.

Guinier, A. 1963. X-ray Diffraction in Crystals, Imperfect Crystals, and Amorphous Bodies. W. H. Freeman, San Francisco. 295–309.

Gulik-Krzywicki, T. 1975. Structural studies of the associations between biological membrane components. *Biochim. Biophys. Acta.* 415:1–28.

Henderson, R. 1975. The structure of the purple membrane from *Halobacterium halobrium*: analysis of the x-ray diffraction pattern. *J. Mol. Biol.* 93:123–138.

Herbette, L., J. Marquardt, A. Scarpa, and J. K. Blasie. 1977. A direct analysis of lamellar x-ray diffraction from hydrated oriented multilayers of fully functional sarcoplasmic reticulum. *Biophys. J.* 20:245–272.

Hui, S. W., and T. P. Stewart. 1981. "Lipid particles" are intermembrane attachment sites. Reply by A. J. Verkleij and B. DeKruijff. *Nature (Lond.)*. 290:427–428.

Levine, Y. K. 1973. X-ray diffraction studies of membranes. *Prog. Surf. Membr. Sci.* 3 (part 4):279–352.

Litman, B. J. 1979. Rhodopsin: its molecular substructure and phospholipid interactions. *Photochem. Photobiol.* 29:672–677.

Luzzati, V. 1968. X-ray diffraction studies of lipid-water systems. *In* Biological Membranes. I. D. Chapman, editor. Academic Press, Inc., London. 71–202.

Michel-Villaz, M., H. R. Saibil, and M. Chabre. 1979. Orientation of rhodopsin α-helices in retinal rod outer-segment membranes studied by infrared linear dichroism. *Proc. Natl. Acad. Sci. U. S. A.* 76:4405–4408.

Miljanich, G. P., P. P. Nemes, D. L. White, and E. A. Dratz. 1981. The asymmetric transmembrane distribution of phosphatidylethanolamine,

phosphatidylserine and fatty acids of the bovine retinal rod outer segment disk membrane. *J. Membr. Biol.* 60:249–255.

Nelander, J. C., and A. E. Blaurock. 1978. Disorder in nerve myelin: phasing the higher order reflections by means of the diffuse scatter. *J. Mol. Biol.* 118:497–532.

Olive, J. 1980. The structural organization of mammalian retinal disc membrane. *Int. Rev. Cytol.* 64:107–169.

Osborne, H. B., and E. Nabedryk-Viala. 1977. The hydrophobic heart of rhodopsin revealed by an infrared ^{1}H-^{2}H exchange study. *FEBS (Fed. Eur. Biochem. Soc.) Lett.* 84:217–220.

Quinn, P. J., and D. Chapman. 1980. The dynamics of membrane structure. *CRC Crit. Rev. Biochem.* 8:1–117.

Raubach, R. A., P. P. Nemes, and E. A. Dratz. 1974. Chemical labeling and freeze fracture studies on localization of rhodopsin in rod outer segment disk membranes. *Exp. Eye Res.* 18:1–12.

Raviola, G., and E. Raviola. 1981. Paracellular root of aqueous outflow in the trabecular meshwork end canal of Schlemm. *Invest. Ophthalmol. Visual Sci.* 21:52–72.

Reynolds, Geo. T., and J. Milch. 1976. Image tube characteristics of importance in x-ray diffraction studies. *Adv. Electronics and Elec. Phys.* 40*B*:923–943.

Reynolds, Geo. T., J. Milch, and S. Gruner. 1977. Image intensification of x-ray diffraction patterns from biological structures. *IEEE Trans. Nuc. Sci.* NS-24:501–510.

Reynolds, Geo. T., J. R. Milch, and S. M. Gruner. 1978. A high sensitivity image intensifier-TV detector for x-ray diffraction studies. *Rev. Sci. Instrum.* 49:1241–1249.

Rothschild, K. J., J. R. Andrew, W. J. DeGrip, and H. E. Stanley. 1976. Opsin structure probed by Raman spectroscopy of photoreceptor membranes. *Science (Wash., D. C.).* 191:1176–1178.

Rothschild, K. J., W. J. DeGrip, and R. Sanches. 1980 *a*. Fourier transform infrared study of photoreceptor membrane. *Biochim. Biophys. Acta.* 596:338–351.

Rothschild, K. J., K. M. Rosen, and N. A. Clark. 1980 *b*. Incorporation of photoreceptor membrane into a multilamellar film. *Biophys. J.* 31:45–52.

Rothschild, K. J., R. Sanches, T. L. Hsiao, and N. A. Clark. 1980 *c*. A spectroscopic study of rhodopsin alpha-helix orientation. *Biophys. J.* 31:53–64.

Santillan, G. 1975. An x-ray diffraction study of isolated retinal photoreceptor disk membranes: the structure of water-washed disk membranes in dark-adapted and bleached states at 8 Å resolution. Ph.D. Thesis. University of Pennsylvania, Philadelphia, PA.

Schnetkamp, P. P. M. 1980. Ion selectivity of the cation transport system of isolated intact cattle rod outer segments. Evidence for a direct communication between the rod plasma membrane and the rod disk membranes. *Biochim. Biophys. Acta.* 598:66–90.

Schwartz, S., J. E. Cain, E. Dratz, and J. K. Blasie. 1975. An analysis of the lamellar x-ray diffraction from disordered membrane multilayers with applications to data from retinal rod outer segments. *Biophys. J.* 15:1201–1232.

Shipley, G. G. 1973. Recent x-ray diffraction studies of biological membranes and membrane components. *In* Biological Membranes. D. Chapman, and D. F. H. Wallach, editors. Academic Press, Inc., NY. Vol. 2.

Wunderlich, F., A. Ronai, V. Speth, J. Seelig, and A. Blume. 1975. Thermotropic lipid clustering in tetrahymena membranes. *Biochemistry.* 14:3730–3735.

Young, R. W. 1974. Biogenesis and renewal of visual cell outer segment membranes. *Exp. Eye Res.* 18:215–223.